Journal of the Serbian Chemical Society
JSCS-info@shd.org.rs • www.shd.org.rs/JSCS

ACCEPTED MANUSCRIPT

Journal of the Serbian Chemical Society
JSCS-info@shd.org.rs • www.shd.org.rs/JSCS
J. Serb. Chem. Soc. **00(0)** 1-16 (2024)
JSCS–12799
Original scientific paper
Published DD MM, 2024

Investigation of adsorption properties of SF_6 decomposed gases (SO_2 and SO_2F_2) on pristine and Ti-decorated SWCNT surfaces: A DFT study

ELHAM GHOLAMREZAI KOHAN[1], HOSSEIN MOHAMMADI-MANESH[1*], FOROUGH KALANTARI FOTOOH[2]

[1]*Department of Chemistry, Faculty of Science, Yazd University, Yazd, Iran, and* [2]*Department of Chemistry, Yazd Branch, Islamic Azad University, Yazd, Iran*

(Received 2 February; revised 1 March; accepted 17 April 2024)

Abstract: DFT calculations were employed to investigate the adsorption of gases produced from SF_6 decomposition (SO_2 and SO_2F_2) on pristine and Ti-decorated single-walled carbon nanotubes (Ti-(8, 0) SWCNT). All structures were relaxed and their structural and electronic properties were investigated before and after gas adsorption on the surface of the nanotubes. (Ti-(8, 0) SWCNT) was found to have high chemisorption sensitivity to Ti, SO_2F_2, and SO_2 adsorptions on its surface. The electronic properties of (8, 0) SWCNT were altered from semiconductor to metallic upon decoration with Ti, as demonstrated by calculated band structures and density of states (DOS). SO_2F_2 and SO_2 adsorption on the surface of (Ti-(8, 0) SWCNT) from different sides transformed the conductor (Ti-(8, 0) SWCNT) into a semiconductor nanotube. To more carefully study the nature of adsorption, partial density of states (PDOS) calculations were also made. Additionally, Ti decoration induced a magnetization of approximately 2.61 μB in (8, 0) SWCNT, which disappeared after gas adsorption.

Keywords: gas adsorption; carbon nanotube; modified nanotube; electronic properties; charge transfer.

INTRODUCTION

Sulfur hexafluoride (SF_6) has been widely used in gas-insulated equipment, but it can decompose into SO_2F_2, SO_2, and other compounds[1] under partial discharge over time. Various methods, such as gas chromatography and detector tubes,[2] have been used to identify SF_6 decomposition products. Since carbon nanotube discovery in 1991,[3] it has been been widely used in nanotechnology, energy storage materials, gas adsorption properties,[4] and hydrogen storage.[5] In addition to their essential applications, numerous studies have focused on

* Corresponding author. E-mail: mohammadimanesh@yazd.ac.ir
https://doi.org/10.2298/JSC240202047K

preparing CNTs for gas detection due to their excellent properties, including higher sensitivity, faster response, and the ability to detect a wider variety of gases. To improve the detection properties of CNTs, various methods have been proposed, including decorating or doping them with metal atoms to enhance their functionality in identifying a wide range of gases.[6] Kong *et al.* have reported the gas sensing properties of single-walled CNTs, laying the groundwork for the application of one-dimensional nanomaterials in gas detection.[7] Zhao *et al.* have studied the adsorption of N_2 gas and various gas molecules on (5, 5) SWCNTs and bundles using DFT. They observed weak interactions between SWCNTs and gas molecules, which did not significantly influence the electronic structures of carbon nanotubes.[8] In another study, Zhou *et al.* have investigated the adsorption of SO_2, CH_3OH, and CH_4 on Pd-decorated (5, 5) CNTs. The strong binding energies and significant electron charge transfers indicated the promising potential of Pd-CNTs for detecting these gas molecules.[9] Ozekmekci *et al*. investigated the adsorption of hydrogen sulfide onto gallium (Ga), germanium (Ge) and boron (B) doped (4, 0) single-walled carbon nanotubes (SWCNTs) using DFT. Their results showed that all doped SWCNT structures have negative Gibbs free energy and adsorption energy values, indicating their potential for H_2S removal via adsorption.[10] patrignani *et al*. studied the adsorption of NO and CO on pristine and metal-decorated (8, 0) SWCNT using DFT. Both gases caused a slight deformation of the nanotube curvature in the direction of the adsorbed molecule. Their research demonstrated that decorating SWCNTs with transition metals (Sc, Cr, Fe, and Ni) enhances both molecule adsorption and sensing performance.[11] The selection of the (8, 0) zigzag SWCNT is driven by its semiconducting properties and heightened sensitivity to conductivity changes, making it a preferred choice for gas detection.[12] Furthermore, an increase in the tube diameter results in a smaller broken symmetry factor (larger n), thereby enhancing the adsorption capability of the SWCNT.[13] Recently experimental and theoretical simulations have indicated the potential for uniform coating of carbon nanotubes with Ti atoms. The nearly empty d orbitals of Ti facilitate interactions with ligands such as gases. Consequently, charge transfer occurs from the ligands highest occupied orbital to the empty orbital in Ti. This is followed by a reverse charge donation from the d orbital back to the ligand's lowest unoccupied orbital. This intricate charge transfer process, along with covalent bonding with Ti, leads to the formation of a stable Ti-C bond.[14] It's noteworthy that there is a dearth of reports concerning the utilization of Ti-decorated carbon nanotubes for detecting SF_6 decomposition products in gas insulation equipment. Thus, this study holds significant importance as it offers fresh insights into the development of gas sensors through the utilization of Ti-decorated SWCNTs for this specific purpose. In this study, we investigate the gas sensing properties of (8, 0) SWCNT and Ti-decorated (8, 0) SWCNT for SF_6 decomposed gases (SO_2F_2 and SO_2) using DFT calculations. We analyze the

structural parameters, adsorption energies, density of states (DOS), band structures, and partial density of states (PDOS) to describe the interaction between the gases and SWCNTs.

COMPUTATIONAL METHOD

The adsorption of SO_2 and SO_2F_2 molecules to the surfaces of both pristine and Ti-decorated (8, 0) SWCNTs was calculated using the Quantum-Espresso software package.[15] The GGA-PBE functional was used to account for exchange-correlation effects.[16] A typical (8, 0) SWCNT was created in a supercell with lattice constants a = 26.46 Å and c = 4.26 Å. The Monkhorst-Pack scheme with a 1 × 1 × 10 k-point grid was used to sample the Brillouin-zone.[17] An energy cutoff of 60 Ry was set for the wave function in all structures. The VdW-Grimme-D2 approach was used to correct van-der Waals interactions in the calculations. The Xcrysden software was used to display the geometries obtained from DFT calculations. In this study, SO_2 and SO_2F_2 molecules were adsorbed on different sides of the (8, 0) SWCNT and Ti-decorated (8, 0) SWCNT. The structural and electronic properties, such as band structures, density of states (DOS), and partial density of states (PDOS), were calculated. Furthermore, magnetization was assessed through spin-polarized calculations. To investigate the stability of (Ti-(8, 0) SWCNT) structure, the formation energy for Ti adsorbed on the surface of (8, 0) SWCNT is defined as:

$$E_f = E_{Ti/swcnt} - E_{swcnt} - E_{Ti} \quad (1)$$

Where $E_{Ti/swcnt}$, E_{Ti}, and E_{Ti} are total energies of the Ti-SWCNT, isolated SWCNT, and isolated Ti atom, respectively. The adsorption energy is computed to describe the gas-surface interaction:[18]

$$E_{ads} = E_{surface/gas} - E_{surface} - E_{gas} \quad (2)$$

Where the parameter $E_{surface/gas}$ represents the total energy of adsorbed structures, $E_{surface}$ and E_{gas} are the energies of optimized pristine or Ti decorated (8, 0) SWCNT and the isolated gas molecules, respectively. Based on Eq. (2), negative values with greater absolute values of adsorption energy indicate favorable adsorptions. We utilized Bader charge analysis[19,20] for a comprehensive understanding of the gas adsorption mechanism. Charge transfer between Ti and SWCNT is determined by the equation:

$$Q_t = Q_{Ti/swcnt} - Q_{Ti} \quad (3)$$

Where $Q_{Ti/swcnt}$ and Q_{Ti} represent the charge transfer for the Ti decorated on SWCNT and isolated Ti, respectively. The charge transfer for each gas adsorption process is calculated as:

$$Q_g = Q_{gas/surface} - Q_{gas} \quad (4)$$

Here $Q_{gas/surface}$ and Q_{gas} denote the charge transfer amount after adsorption by the gas and isolated gas, respectively. A negative value of charge transfer indicates the acceptance of electrons by the gas molecules.

RESULTS AND DISCUSSION

Adsorption of SO_2 to pristine (8, 0) SWCNT

The optimized structure of the pristine (8, 0) SWCNT with the number of carbon atoms is depicted in Figure 1. As shown in Figure 1, after optimization, the

C1-C2 and C1-C3 bond lengths of the (8, 0) SWCNT are approximately 1.43 and 1.42 Å, respectively, which are consistent with previous findings.[21]

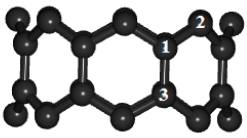

Fig. 1. The optimized structure of pristine (8, 0) SWCNT.

The SO_2 molecule was added in front of the C1 atom of the nanotube from both S and O sides. To distinguish between them, SO_2-S-CNT is used when SO_2 is adsorbed from the S side, and SO_2-O-CNT is utilized when SO_2 is adsorbed from the O side. Fig. 2 shows the optimized configurations of SO_2-S-CNT and SO_2-O-CNT.

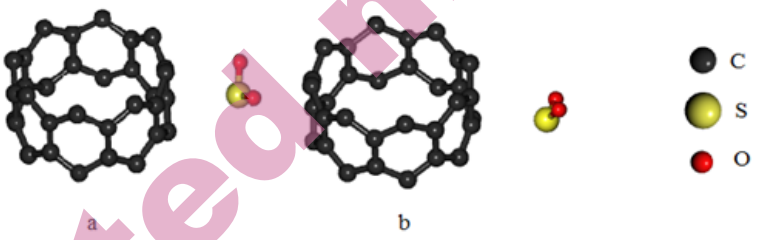

Fig. 2. The optimized configurations of SO_2-S-CNT a) and SO_2-O-CNT b).

From Fig. 2, it is apparent that the SO_2 molecule is situated at a considerable distance from the (8, 0) SWCNT in SO_2-S-CNT and SO_2-O-CNT configurations, with distances of 3.04 and 3.28 Å, respectively. The adsorption energies of SO_2 in SO_2-S-CNT and SO_2-O-CNT configurations are -0.24 and -0.23 eV, respectively. Table I presents the nearest bonding distances (D) and adsorption energies of all structures. Low adsorption energy values and long distances suggest weak adsorption of SO_2 to the (8, 0) SWCNT in both configurations. Band structures and DOSs of each structure are illustrated in Fig. 4. Black and red lines in Fig. 4 indicate spin up and spin down bands, respectively. The results confirm that (8, 0) SWCNT is a semiconductor with a band gap of 0.59 eV, consistent with previous studies.[22] Upon SO_2 adsorption, a new band emerges above the Fermi level in the conduction band of both configurations which can be attributed to p orbitals of S and O atoms of the SO_2 molecule (Figs. 4b and 4c). However, the band gaps do not change significantly after adsorption, as seen in Table I. All structures exhibit overlapping of spin up and spin down bands, indicating no induced magnetization after SO_2 adsorption from both sides. To gain further insight into the nature of adsorption, the partial densities of states (PDOSs) are presented in Fig. 5. The left

and right sides of each graph show the spin up and spin down PDOSs, respectively. From Figs. 5b and 5c, it is observed that p orbitals of S and O atoms in SO_2 have high density at about -7 eV and are hybridized with p orbitals of the carbon atom in (8, 0) SWCNT. However, this hybridization is far from the Fermi level and does not result in bond formation in either configuration. Therefore, the adsorption of SO_2 does not significantly alter the magnetic or electronic properties of (8, 0) SWCNT, which is in consistent with previous findings.[22] For visualizing electronic distribution, Bader charge analyses calculated the charge difference before and after gas adsorption on nanotube surfaces. The charge transfer for all configurations was computed using Eq. (4) and is presented in Tables I and II. As indicated in Table I, no significant electron transfers were observed between SO_2 gas and (8, 0) SWCNT in SO_2-S-CNT and SO_2-O-CNT configurations.

Adsorption of SO_2F_2 to (8, 0) SWCNT

The optimized configurations of SO_2F_2-F-CNT and SO_2F_2-O-CNT, which represent the adsorption of the SO_2F_2 molecule to the SWCNT from F and O sides, respectively, are shown in Fig. 3.

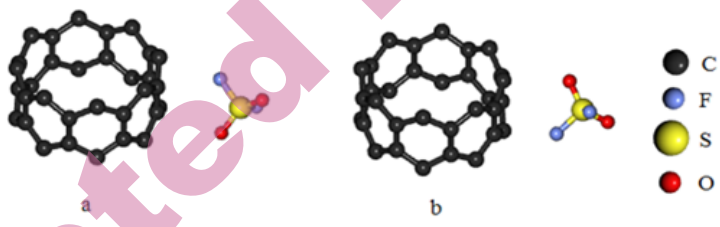

Fig. 3. The optimized configurations of (8, 0) SWCNT after SO_2F_2 adsorption a) from F side (SO_2F_2-F-CNT) b) from O side (SO_2F_2-O-CNT).

The results show that, after optimization, the SO_2F_2 molecule is located at a distance of 3.22 and 3.19 Å from the CNT in SO_2F_2-F-CNT and SO_2F_2-O-CNT configurations, respectively. Table I displays the adsorption energies and the nearest distance (D) between SO_2F_2 and the C atom of (8, 0) SWCNT. The results reveal that the adsorption energy of SO_2F_2 is more negative than that of SO_2, favoring SO_2F_2 adsorption over SO_2 onto SWCNT. Nevertheless, the conjunction of extended distances and low adsorption energies suggests a weak adsorption. Fig. 4 shows the band structure and DOS results of SO_2F_2 adsorption on SWCNT. The conduction band of the system displays new energy levels that are far from the Fermi level and do not significantly affect the band gap. The PDOS of these structures are also illustrated in Fig. 5. Spin up and spin down peaks for both configurations are symmetric which can be attributed to non-magnetic nature of these structures. Our PDOS findings demonstrate that p orbitals of O and F atoms of SO_2F_2 in both configurations are located far from the Fermi level, and cannot hybridize with p orbital of carbon atom in the (8, 0) SWCNT, located near the

Fermi level. This reinforces the conclusion that SO_2F_2 adsorption is weak, as suggested by our electronic calculations. Charge analyses in Table I reveal minimal charge transfer from SO_2F_2 gas to the surface of (8, 0) SWCNT in both SO_2F_2-F-CNT and SO_2F_2-O-CNT configurations. Thus, electronic calculations substantiate the notion that SO_2F_2 adsorption onto (8, 0) SWCNT is weak.

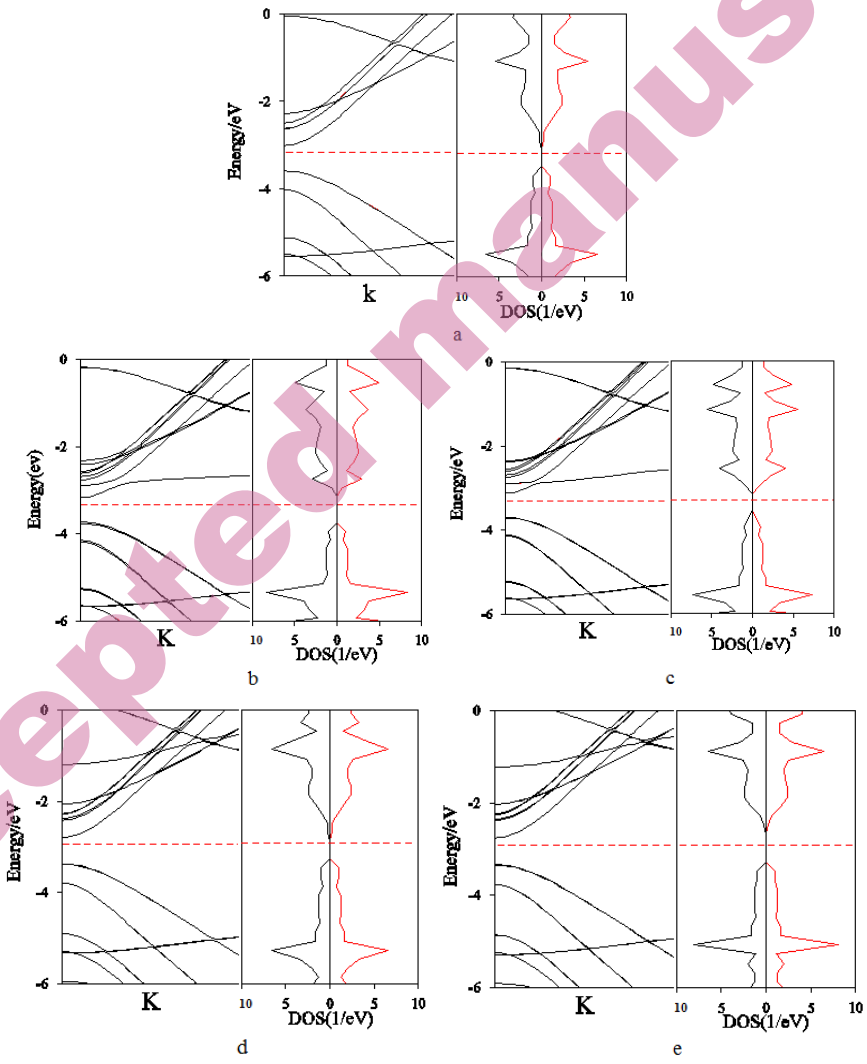

Fig. 4. Band structure and DOS of a) (8, 0) SWCNT before adsorption b) after SO_2 adsorption from S side (SO_2-S-CNT) c) after SO_2 adsorption from O side (SO_2-O-CNT) d) after SO_2F_2 adsorption from F side (SO_2F_2-F-CNT) and e) after SO_2F_2 adsorption from O side (SO_2F_2-O-CNT). Black and red lines show spin up and spin down bands, respectively. Red dash line shows the Fermi level.

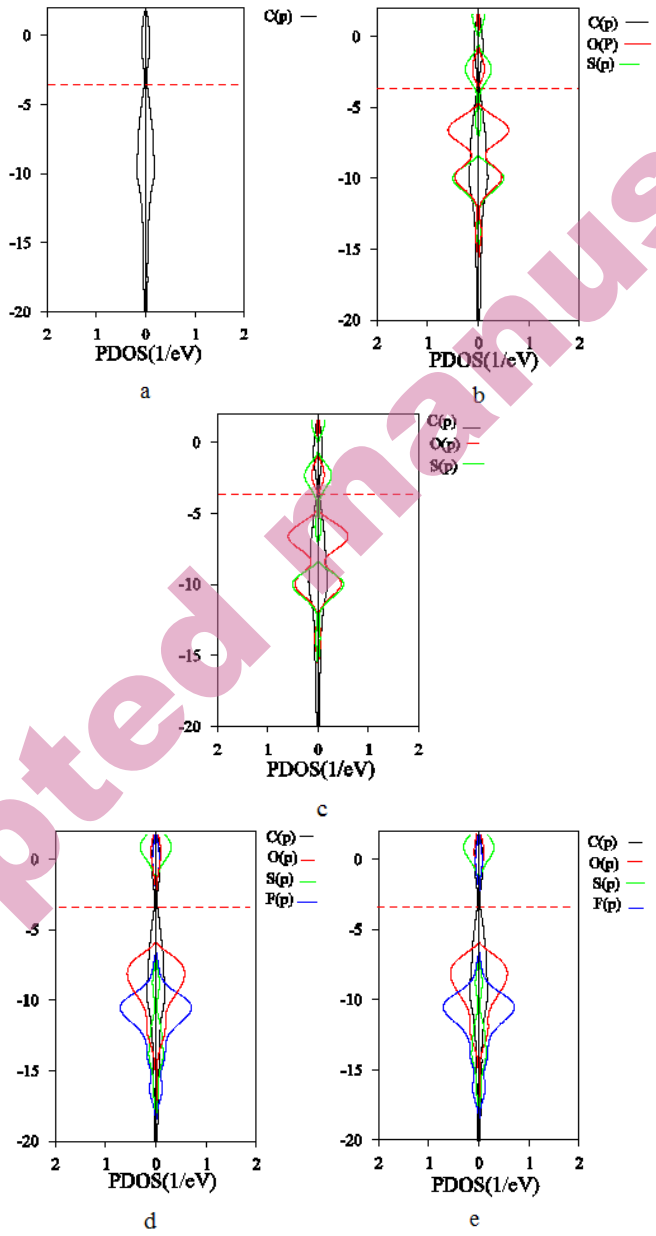

Fig. 5. PDOS of a) (8, 0) SWCNT before adsorption b) after SO_2 adsorption from S side (SO_2-S-CNT) c) after SO_2 adsorption from O side (SO_2-O-CNT) d) after SO_2F_2 adsorption from F side (SO_2F_2-F-CNT) and e) after SO_2F_2 adsorption from O side (SO_2F_2-O-CNT). Left and right side of each graph show the spin up and spin down bands, respectively. Red dash line shows the Fermi level.

TABLE I. Nearest atoms and their distances (D), adsorption energies (E_{ads}), band gaps (E_g), magnetization (μ) of (8, 0) SWCNT before and after gas adsorption and Bader charge analysis for all configurations (Q_g)

Configuration	to	D	E_{ads} / eV	E_g / eV	μ	Q_g
SWCNT				0.59	0	
SO_2-S-CNT	C-S	3.04	-0.24	0.56	0	-0.05
SO_2-O-CNT	C-S	3.28	-0.23	0.57	0	-0.07
SO_2F_2-F-CNT	C-F	3.22	-0.79	0.58	0	-0.01
SO_2F_2-O-CNT	C-O	3.19	-0.78	0.58	0	-0.01

Adsorption of SO_2 to Ti-(8, 0) SWCNT

Fig. 6a shows the optimized structure of a Ti-decorated (8, 0) SWCNT. Initially, the Ti atom was located in front of the C1 atom of the nanotube at the equilibrium C-Ti distance. As seen in Fig. 6a, the Ti atom moves to the hollow part of the CNT after optimization, in agreement with prior studies.[23] The nearest distance between C atom of the nanotube and Ti atom after optimization is approximately 2.19 Å. The formation energy, calculated using Eq. (1), is about -1.65 eV, confirming the stability of this modified nanotube. The SO_2 molecule was then adsorbed to this modified nanotube from the S and O sides, resulting in SO_2-S-Ti-CNT and SO_2-O-Ti-CNT configurations, respectively.

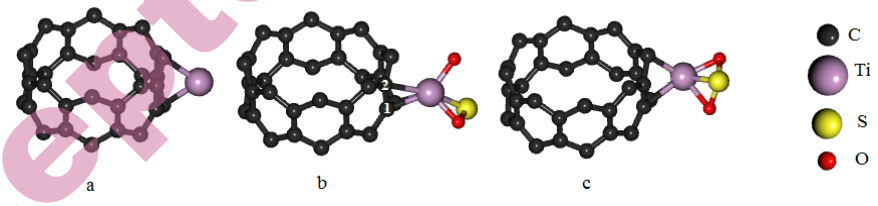

Fig. 6. The optimized configurations of a) Ti-CNT before adsorption b) after SO_2 adsorption from S side (SO_2-S-Ti-CNT) and c) after SO_2 adsorption from O side (SO_2-O-Ti-CNT).

The band structures and DOSs of the (Ti-(8, 0) SWCNT) structure are presented in Fig. 8a. The results indicate that the decoration of titanium on the surface of (8, 0) SWCNT results in the appearance of new bands near the Fermi level, leading to a transition from a semiconductor to a metallic carbon nanotube. The density of states increase near the Fermi level, consistent with earlier findings.[24] The splitting of spin up and spin down bands near the Fermi level induces a magnetization of about 2.61 μB in (Ti-(8, 0) SWCNT). By calculating both the magnetization and conductivity of this structure, it is possible to identify the adsorption of Ti on the surface of (8, 0) SWCNT. Fig. 9a displays the PDOS of (Ti-(8, 0) SWCNT), showing that the s and d orbitals of the Ti atom are

unsymmetrical and lead to the magnetization of the Ti-decorated (8, 0) SWCNT. These orbitals are hybridized with p orbitals of C atom of (8, 0) SWCNT at the Fermi level, resulting in the formation of a Ti-C bond. Since the carbon atom is more electronegative than titanium, the electrons move towards the carbon atom, leading to a partially filled molecular orbital, as reported previously.[23] Bader charge analysis, for Ti and SWCNT charge transfer (calculated using Eq. 3), reveals a significant positive excess charge of +0.86e on the bonded Ti atom. These findings substantiate the concept of charge transfer from the bonded Ti atom to the SWCNT, consistent with earlier investigations.[23,24] Therefore, Ti atom creates active sites that promote surface chemical reactions and support faster sensing. All molecules are bonded to the surface through the Ti atom of (Ti-(8, 0) SWCNT), which is a more suitable adsorption site than other atoms for gas adsorption. The optimized structures of (Ti-(8, 0) SWCNT) after the adsorption of SO_2 from both sides are shown in Fig. 6, and the corresponding parameters and adsorption energies are illustrated in Table II. As depicted in Fig. 6b, after SO_2 adsorption from S side in SO_2-S-Ti-CNT configuration, Ti atom moves to the center of the C1-C2 bond, and the C1-C2 bond length increases from 1.46 Å in Ti-(8, 0) SWCNT to 1.54 Å. The results reveal that after adsorption, one O atom dissociates from the adsorbed molecule. The distance between the Ti and separated O atom of SO_2 is approximately 1.93 Å, while the Ti atom is bonded to both O and S of OS at distances of 1.90 and 2.35 Å, respectively. In SO_2-O-Ti-CNT configuration, the Ti atom remains above the hollow site of (8, 0) SWCNT. The results show that in this configuration, the Ti atom is bonded to all three atoms of the SO_2 molecule. The nearest distance between the Ti atom of (Ti-(8, 0) SWCNT) and the O atom of SO_2 is 1.93 Å. In both configurations, the O atoms are close to the Ti atom, which can be attributed to the strong electronegativity of the oxygen atom, in agreement with previous reports.[25] Due to the strong interaction between the Ti atom and the dissociated O atom of SO_2 in SO_2-S-Ti-CNT configuration, it can be concluded that more electrons transfer from (Ti-(8, 0) SWCNT) to the SO_2 molecule in this configuration than in SO_2-O-Ti-CNT configuration, consistent with previous works.[26] Table II displays the adsorption energies of SO_2 in SO_2-S-Ti-CNT and SO_2-O-Ti-CNT configurations as -4.77 and -3.58 eV, respectively. The results suggest that SO_2 adsorption from S side is energetically more favored in SO_2-S-Ti-CNT configuration compared to SO_2-O-Ti-CNT configuration. These adsorption energies are more negative than those in pristine SWCNT. The band structures and DOSs of SO_2 adsorption to (Ti-(8, 0) SWCNT) are illustrated in Fig. 8. After SO_2 adsorption, it appears that the half-occupied levels of (Ti-(8, 0) SWCNT) shift up to the conduction band due to electron transfers from the Ti atom to the SO_2 molecule. The band gap of (Ti-(8, 0) SWCNT) is increased to 0.43 and 0.52 eV in SO_2-S-Ti-CNT and SO_2-O-Ti-CNT configurations, respectively. The spin up and spin down levels overlap, indicating no magnetic character in these

configurations. For further comparison, the PDOSs of SO_2 adsorption in SO_2-S-Ti-CNT and SO_2-O-Ti-CNT configurations are presented in Figs. 9b and 9c, respectively. In SO_2-S-Ti-CNT configuration, the d orbitals of the dissociated O atom of the SO_2 molecule have a high density at the Fermi level, confirming more electron transfer in SO_2-S-Ti-CNT configuration than in SO_2-O-Ti-CNT configuration. After SO_2 adsorption, the d orbitals of the Ti atom are presented at the Fermi level and are hybridized with p orbitals of O and S atoms of the SO_2 molecule, which leads to chemical adsorption in both configurations. The comparison of Figs. 9b and 9c with 9a shows that the polarization of Ti orbitals is removed, confirming the electron transfer from Ti atom to the SO_2 molecule. Therefore, SO_2 adsorption alters both the electronic properties and magnetism of (Ti-(8, 0) SWCNT). The Bader charge analysis results are presented in Table II. The analysis reveals more substantial electron transfer in the SO_2-S-Ti-CNT configuration compared to the SO_2-O-Ti-CNT configuration. The negative value of Q_g for SO_2 adsorption in both configurations signifies electron transfer from the (Ti-(8, 0) SWCNT) to SO_2 molecule.

Adsorption of SO_2F_2 to Ti-(8, 0) SWCNT

SO_2F_2 molecule was adsorbed to Ti-modified nanotube from F and O sides, referred to as SO_2F_2-F-Ti-CNT and SO_2F_2-O-Ti-CNT, respectively. The optimized configurations of the (Ti-(8, 0) SWCNT) after the adsorption of SO_2F_2 from both sides are depicted in Fig. 7.

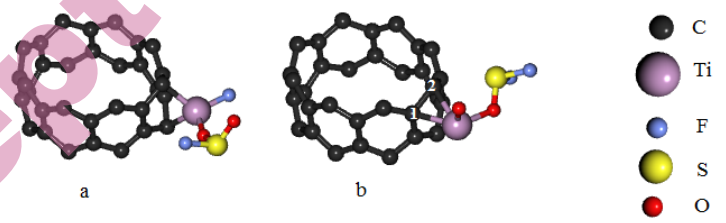

Fig. 7. The optimized configurations of Ti-decorated (8, 0) SWCNT after SO_2F_2 adsorption a) from F side (SO_2F_2-F-Ti-CNT) b) from O side (SO_2F_2-O-Ti-CNT).

In SO_2F_2-F-Ti-CNT configuration, the Ti atom remains above the hollow site of the (Ti-(8, 0) SWCNT), as shown in Fig. 7a. The C-Ti bond length decreases from 2.19 Å in the (Ti-(8, 0) SWCNT) to 2.09 Å. The results indicate that after adsorption, one F atom dissociates from the adsorbed molecule. This dissociative adsorption is similar to the adsorption of SO_2F_2 to the PtN_3-CNT surface.[27] The distance between the Ti atom and the separated F atom of SO_2F_2 is approximately 1.77 Å. The Ti atom forms a bond with O atom of SO_2F at a distance of 1.85 Å. In SO_2F_2-O-Ti-CNT configuration, after adsorption of SO_2F_2 from O side, Ti atom moves to the center of the C1-C2 bond, as depicted in Fig.7b. This causes an

increase in the C1-C2 bond length from 1.46 Å in (Ti-(8, 0) SWCNT) to 1.52 Å, thereby increasing the orbital overlap after adsorption. The results indicate that after adsorption, one O atom dissociates from the adsorbed molecule. Therefore, a strong bond is formed. The distance between the Ti atom and separated O atom of SO_2F_2 is approximately 1.68 Å. The Ti atom forms a bond with the O atom of SO_2F at a distance of 2.08 Å. The adsorption energies in both configurations and the nearest distance between SO_2F_2 and the Ti atom of (Ti-(8, 0) SWCNT) (D) are presented in Table II High adsorption energies and dissociation of SO_2F_2 post-adsorption in both configurations imply robust adsorption, aligning with prior reports.[24] The results demonstrate that the SO_2F_2 adsorption energy in SO_2F_2-F-Ti-CNT configuration is more negative than in SO_2F_2-O-Ti-CNT configuration, which can be attributed to the dissociated F atom and its higher electronegativity in SO_2F_2-F-Ti-CNT configuration. Fig. 8 shows the DOS and band structures of SO_2F_2 adsorption on (Ti-(8, 0) SWCNT). As depicted in Fig. 8d, when SO_2F_2 is adsorbed to (Ti-(8, 0) SWCNT) from F side in SO_2F_2-F-Ti-CNT configuration, the Fermi level shifts down, and two bands near the Fermi level shift up to the conduction band, which can be attributed to the d orbitals of the Ti atom. The conductor Ti-decorated nanotube changes to a semiconductor nanotube with a band gap of 0.30 eV and no magnetic property after adsorption. On the other hand, when SO_2F_2 is adsorbed to (Ti-(8, 0) SWCNT) from O side in SO_2F_2-O-Ti-CNT configuration, the DOS at the Fermi level approaches zero, and the band gap increases to 0.50 eV (refer to Fig. 8e for band structure and DOS). The PDOSs of SO_2F_2 adsorption in SO_2F_2-F-Ti-CNT and SO_2F_2-O-Ti-CNT configurations are illustrated in Figs. 9d and 9e, respectively. Comparison of Figs. 9d and 9e reveals that the p orbitals of the dissociated F atom in SO_2F_2-F-Ti-CNT configuration have high density at the Fermi level, whereas the valence orbitals of the dissociated O atom in SO_2F_2-O-Ti-CNT configuration have low density at the Fermi level. This confirms the stronger interaction between (Ti-(8, 0) SWCNT) and SO_2F_2 gas in SO_2F_2-F-Ti-CNT configuration. The spin up and spin down electronic states overlap in both configurations of SO_2F_2, and no magnetization can be observed in these configurations. The valence orbitals of all atoms of the SO_2F_2 molecule also appear at the Fermi level and are hybridized with the high-intensity peaks of the Ti atom, which leads to chemical bond formation in these configurations. Bader charge analysis reveals greater charge transfer in the SO_2F_2-F-Ti-CNT configuration compared to SO_2F_2-O-Ti-CNT, as shown in Table II. The negative charge transfer value for SO_2F_2 adsorption in both configurations indicates electron donation from the (Ti-(8, 0) SWCNT) to gas molecule.

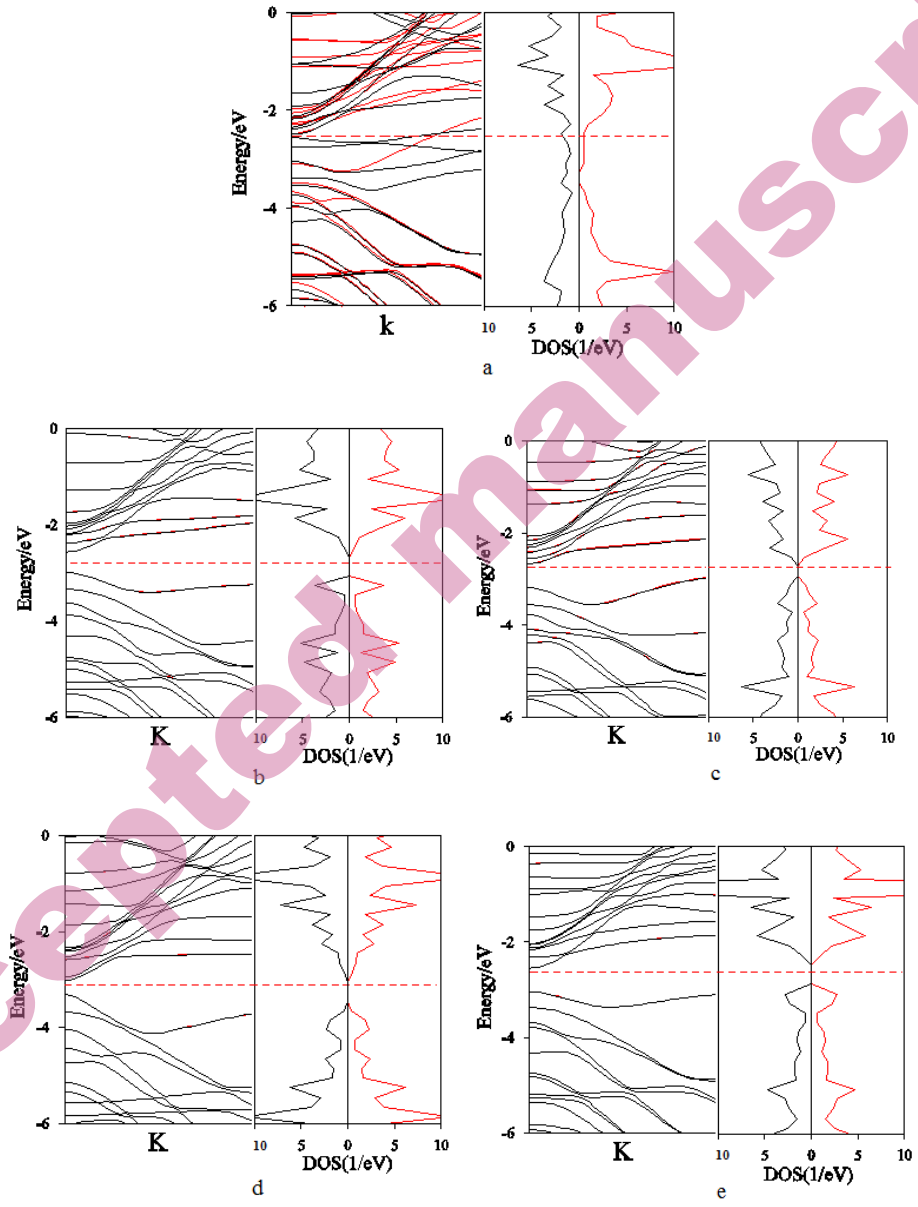

Fig. 8. Band structure and DOS of a) Ti-SWCNT before adsorption b) after SO_2 adsorption from S side (SO_2-Ti-S-CNT) c) after SO_2 adsorption from O side (SO_2-O-Ti-CNT) d) after SO_2F_2 adsorption from F side (SO_2F_2-F-Ti-CNT) and e) after SO_2F_2 adsorption from O side (SO_2F_2-O-Ti-CNT). Black and red lines show spin up and spin down bands, respectively. Red dash line shows the Fermi level.

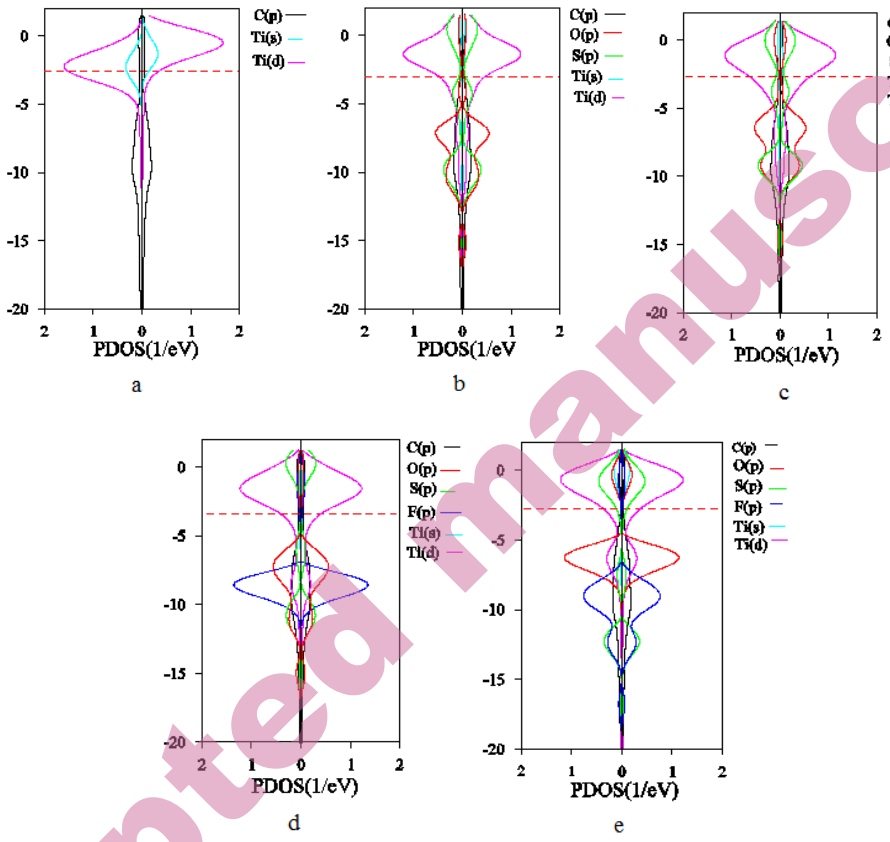

Fig. 9. PDOS of a) Ti-SWCNT before adsorption b) after SO_2 adsorption from S side (SO_2-S-Ti-CNT) c) after SO_2 adsorption from O side (SO_2-O-Ti-CNT) d) after SO_2F_2 adsorption from F side (SO_2F_2-F-Ti-CNT) and e) after SO_2F_2 adsorption from O side (SO_2F_2-O-Ti-CNT). Left and right side of each graph show the spin up and spin down bands, respectively. Red dash line shows the Fermi level.

TABLE II. Formation energies (E_f), nearest atoms and their distances (D), adsorption energies (E_{ads}), band gaps (E_g), magnetization (μ) of (Ti-(8, 0) SWCNT) before and after gas adsorption and Bader charge analysis for all configurations (Q_g)

Configuration	E_f / eV	to	D	E_{ads} / eV	E_g / eV	μ	Q_g
Ti-SWCNT	-1.65	Ti-C	2.19			2.61	
SO_2-S-Ti-CNT		Ti-O	1.90	-4.77	0.43	0	-1.02
SO_2-O-Ti-CNT		Ti-O	1.93	-3.58	0.52	0	-0.95
SO_2F_2-F-Ti-CNT		Ti-F	1.77	-6.74	0.30	0	-1.29
SO_2F_2-O-Ti-CNT		Ti-O	1.68	-5.39	0.50	0	-1.18

CONCLUSION

In this study, we examined the adsorption of gases resulting from the decomposition of SF_6 (SO_2 and SO_2F_2) on the surface of pristine and Ti-decorated (8, 0) SWCNTs from different sides using DFT calculations. The formation energy revealed that Ti-decorated (8, 0) SWCNT is thermodynamically stable. To investigate the interaction between gases and SWCNTs, we calculated the adsorption energy, band structures, density of states, partial density of states (PDOS), magnetic behavior, charge transfer and conductivity. The principal conclusions are as follows:

1. SO_2 and SO_2F_2 weakly adsorb on (8, 0) SWCNT without altering its electronic properties.

2. Decorating (8, 0) SWCNT with titanium shifts electronic properties from semiconducting to metallic, acting as an active site for SF_6 decomposed gas adsorption.

3. Strong adsorption of SO_2 and SO_2F_2 on Ti-(8, 0) SWCNT changes system conductivity from metallic to semiconductor.

4. The conductivity order after SO_2 and SO_2F_2 adsorption on (Ti-(8, 0) SWCNT) from different sides is as follows: SO_2F_2-F-Ti-CNT < SO_2-S-Ti-CNT < SO_2F_2-O-Ti-CNT < SO_2-O-Ti-CNT.

5. The negative charge transfer values for SO_2F_2 and SO_2 adsorptions indicates electron donation from the (Ti-(8, 0) SWCNT) to gas molecules.

Based on the sensing mechanism, (Ti-(8, 0) SWCNT) can be used to prepare a gas chemiresistor sensor for detecting SF_6 decomposed products (SO_2 and SO_2F_2) in SF_6 insulated equipment.

Acknowledgements: The authors would like to acknowledge the support of Yazd University in Iran for providing the computing resources necessary to carry out this research.

И З В О Д

ИСПИТИВАЊЕ ОСОБИНА АДСОРПЦИЈЕ ГАСОВА НАСТАЛИХ РАЗГРАДЊОМ SF_6 (SO_2 И SO_2F_2) НА НЕДИРНУТИМ И Ti-УКРАШЕНИМ SWCNT ПОВРШИНАМА: DFT СТУДИЈА

ELHAM GHOLAMREZAI KOHAN[1], HOSSEIN MOHAMMADI-MANESH[1], FOROUGH KALANTARI FOTOOH[2]

[1]Department of Chemistry, Faculty of Science, Yazd University, Yazd, Iran, и [2]Department of Chemistry, Yazd Branch, Islamic Azad University, Yazd, Iran

DFT израчунавања су искоришћена за истраживање адсорпцију гасова прозведених разградњом SF_6 (SO_2 и SO_2F_2) на недирнутим и Ti-украшеним једнозидним угљеничним наноцевима (Ti-(8, 0) SWCNT). Све структуре су релаксиране и њихове структурне и електронске особине истражене пре и после адсорпције гаса на површини наноцеви. За (Ti-(8, 0) SWCNT) је нађено да има високу хемисорпцијску осетљивост на Ti, SO_2F_2, и SO_2 адсорпције на својој површини. Електронске особине (8, 0) SWCNT су промењене од полупроводничких на металне при украшавању са Ti, како је показано израчунатим структурама трака и густинама стања (DOS). SO_2F_2 и SO_2 адсорпција на површини (Ti-(8, 0) SWCNT) са различитих страна трансформише проводну (Ti-(8, 0) SWCNT) у полопроводну

наноцев. Да би пажљиво испитали природу адсорпције, урађена су и израчунавања парцијалних густина стања (PDOS). Додатно, украшавање са Ti индукује магнетизацију од приближно 2.61 μB у (8, 0) SWCNT, која нестаје након адсорпције гаса.

(Примљено 2. фебруара; ревидирано 1. марта; прихваћено 17. априла 2024.)

REFERENCES

1. I. Sauers, H. W. Ellis, L. G. Christophorou, *IEEE Trans. Elect. Insul.* **2** (1986) 111 (https://doi.org/10.1109/TEI.1986.348932)
2. X. Zhang, B. Yang, W. Liu, J. Zhang, *Procedia Engineering*. **29** (2012) 4107 (https://doi.org/10.1016/j.proeng.2012.01.628)
3. S. Iijima, *Nature* **354** (1991) 56 (https://doi.org/10.1038/354056a0)
4. D. R. Kauffman, A. Star, *Angew. Chem. Int. Ed.* **47** (2008) 6550 (https://doi.org/10.1002/anie.200704488)
5. R. Ströbel, J. Garche, P. T. Moseley, L. Jörissen, G. Wolf, *J. Power Sources* **159** (2006) 781 (https://doi.org/10.1016/j.jpowsour.2006.03.047)
6. S. Demir, M. F. Fellah, *Surf. Sci.* **701** (2020) 121689 (https://doi.org/10.1016/j.susc.2020.121689)
7. J. Kong, N. R. Franklin, C. Zhou, M. G. Chapline, S. Peng, K. Cho, H. Dai, *Science* **287** (2000) 622 (https://doi.org/10.1126/science.287.5453.622)
8. J. Zhao, A. Buldum, J. Han, J. P. Lu, *J. Nanotech.* **13** (2002) 195 (https://doi.org/10.1088/0957-4484/13/2/312)
9. X. Zhou, W. Q. Tian, X. L. Wang, *Sens. Act. B: Chem.* **151** (2010) 56 (https://doi.org/10.1016/j.snb.2010.09.054)
10. G. Gecim, & M. Ozekmekci, *Surf. Sci.* **711** (2021) 121876 (https://doi.org/10.1016/j.susc.2021.121876)
11. M. Patrignani, J. Juan, O. Nagel, W. Reimers, R. Luna, P. V. Jasen, *Pow. Tech.* (2024) 119691 (https://doi.org/10.1016/j.powtec.2024.119691)
12. P. O. Krasnov, T. V. Basova, A. Hassan, *Appl. Surf. Sci*. **457** (2018) 235 (https://doi.org/10.1016/j.apsusc.2018.06.282)
13. W. Li, J. J. Ma, P. Liu, Z. L. Pan, Q. Y. He, *Appl. Surf. Sci*. **335** (2015) 17 (https://doi.org/10.1016/j.apsusc.2015.01.181)
14. L. L. Yu, S. Zhang, Q. Dong, X. Z. Meng, W. Q. Tian, *J. Comput. Theor. Nanosci.* **8** (2011) 1811 (https://doi.org/10.1166/jctn.2011.1887)
15. P. Giannozzi, S. Baroni, N. Bonini, M. Calandra, R. Car, C. Cavazzoni, D. Ceresoli, G. Chiarotti, M. Cococcioni, I. Dabo, A. DalCorso, S. deGironcoli, S. Fabris, G. Fratesi, R. Gebauer, U. Gerstmann, C. Gougoussis, A. Kokalj, M. Lazzeri, L. Martin-Samos, N. Marzari, F. Mauri, R. Mazzarello, S. Paolini, A. Pasquarello, L. Paulatto, C. Sbraccia, S. Scandolo, G. Sclauzero, A. Seitsonen, A. Smogunov, P. Umari, R. M. Wentzcovitch, *J. Phys: Condens. Matter*. **21** (2009) 395502 (https://doi.org/10.1088/0953-8984/21/39/395502)
16. J. P. Perdew, K. Burke, M. Ernzerhof, *J. Phys. Rev. Lett.* **77** (1996) 3865 (https://doi.org/10.1103/PhysRevLett.77.3865)
17. H. J. Monkhorst, J. D. Pack, *J. Phys. Rev. B.* **13** (1976) 5188 (https://doi.org/10.1103/PhysRevB.13.5188)
18. S. F. Boys, F. G. M. P. Bernardi, *J. Mol. Phys.* **19** (1970) 553 (https://doi.org/10.1080/00268977000101561)

19. E. Sanville, S. D. Kenny, R. Smith, G. Henkelman, *J. Comp. Chem.* **28** (2007) 899 (http://doi.org/10.1002/jcc.20575)
20. W. Tang, E. Sanville, G. Henkelman, *J. Phys.: Cond. Matt*. **21** (2009) 084204 (https://doi.org/10.1088/0953-8984/21/8/084204)
21. X. Zhang, Y. Gui, Z. Dai, *Appl. Surf. Sci.* **315** (2014) 196 (https://doi.org/10.1016/j.apsusc.2014.07.056)
22. X. Zhang, J. Zhang, J. Tang, B. Yang, *J. Comp. Theor. Nanosci*. **9** (2012) 1096 (https://doi.org/10.1166/jctn.2012.2149)
23. F. Mei, X. Ma, Y. Bie, G. Xu, *J. Theor. Comp. Chem*. **16** (2017) 1750065 (https://doi.org/10.1142/S0219633617500651)
24. K. W. Kayang, E. Nyankson, J. K. Efavi, V. K. Apalangya, B. I. Adetunji, G. Gebreyesus, A. Yaya, *Res. Phys*. **12** (2019) 2100 (https://doi.org/10.1016/j.rinp.2019.02.062)
25. X. Zhang, Y. Gui, H. Xiao, Y. Zhang, *App. Surf. Sci*. **379** (2016) 47 (https://doi.org/10.1016/j.apsusc.2016.04.048)
26. H. Huang, Y. Yu, M. Zhang, *App. Surf. Sci.* **505** (2020) 144622 (https://doi.org/10.1016/j.apsusc.2019.144622)
27. H. Cui, X. Zhang, D. Chen, J. Tang, *App. Surf. Sci*. **447** (2018) 594 (https://doi.org/10.1016/j.apsusc.2018.03.232).